

Double magnetic phase transitions and magnetotransport anomalies in a new compound Gd_2AgSi_3

Baidyanath Sahu,^{1, a)} R. Djoumessi Fobasso,^{1, b)} and André M. Strydom¹

Highly Correlated Matter Research Group, Physics Department, University of Johannesburg, PO Box 524, Auckland Park 2006, South Africa

Dc and ac-magnetic susceptibility (χ), specific heat (C_P), electrical resistivity (ρ) and magnetoresistance measurements performed on the new polycrystalline compound Gd_2AgSi_3 , crystallizing in the α - ThSi_2 tetragonal structure, are reported. Two magnetic phase transitions were observed in dc and ac susceptibility, specific heat and resistivity measurements at temperatures $T_{N_1} = 11$ K and $T_{N_2} = 20$ K, despite a single site occupied by Gd atom, which is an indication of the complex magnetic behavior. Gd_2AgSi_3 turns out to be one of the rare Gd compound in which a minimum is observed in the temperature dependence of resistivity in the paramagnetic state and also negative magnetoresistance over a wide temperature range (above T_{N_2}), mimicking the behavior of exotic Gd_2PdSi_3 , in this ternary family. The isothermal magnetic entropy change, adiabatic temperature change, and refrigerant capacity reach a value of 9.5 J/kg-K, 7.5 K and 302 J/kg, respectively for the change of magnetic field 9 T.

Keywords: Antiferromagnet, Superzone effect, Magnetoresistance, Magnetocaloric

Rare-earth (RE) based ternary intermetallic compounds have been receiving considerable attention due to their interesting structural, magnetic and physical properties¹⁻⁹. In particular, heavy rare-earth members, which were less considered for a long time in the literature due to the well-localized nature of their 4f-electrons, yielded unique results in the RE_2TX_3 (RE=rare-earth elements, T = transition metals, X = p-block elements) series of compounds. These compounds basically crystallize in the ThSi_2 type of structure which has two modifications namely α - ThSi_2 and β - ThSi_2 phases. Most of the α - ThSi_2 -type of tetragonal structure belongs to a space group of I_4/amd^2 . However, compounds with β - ThSi_2 mostly belong to space group $P6/mmm$ with AlB_2 -type of hexagonal structure. In contrast, Tran¹⁰ has synthesized a series of U_2TGA_3 (T = Ru, Rh, Ir, Pd, Au, Pt) compounds and found that they crystallize in the CeCu_2 type of orthorhombic structure, which belongs to space group *Imma*. Based on different structures, RE_2TX_3 compounds show a variety of magnetic ground states, depending on indirect Ruderman-Kittel-Kasuya-Yosida (RKKY) exchange interaction between the ions. This magnetic interaction dictates the physical properties of the 4f electrons giving rise to interesting and very often anomalous properties^{11,12}.

RE_2TX_3 series of compounds are subject to potential applications in magnetic refrigeration due to the exhibition of large magnetocaloric effect (MCE)¹³⁻¹⁵. MCE-based magnetic refrigeration techniques have attracted considerable attention due to their efficiencies and environmentally friendly nature. The MCE is an intrinsic magneto-thermodynamic phenomena and it describes the change of temperature of the magnetic material when subjected to variable magnetic fields. The

MCE properties of a magnetic material are characterized in terms of isothermal magnetic entropy change (ΔS_m) and adiabatic temperature change (ΔT_{ad}). The refrigeration efficiency of magnetocaloric materials can be considered by evaluating refrigerant capacity (RC), and/or relative cooling power (RCP)¹⁶⁻²³. The MCE of Gd-itself and Gd-based compounds are intensively studied to obtain a good magnetic refrigerant material for their large localised magnetic moments^{13,17,24,25}. In this paper, we attempt to synthesize a new single-phase intermetallic compound Gd_2AgSi_3 . Structural, magnetic, thermal, and electrical transport properties are systematically studied for the present compound. The magnetocaloric effect is extensively investigated from isothermal magnetizations and heat capacity.

A. Synthesis and Experimental Details

A polycrystalline sample of Gd_2AgSi_3 was synthesized by arc-melting the constituent elements of ultra high purity (≥ 99.99 weight %) under an inert Argon gas atmosphere on a water cooled copper hearth. The as-cast ingots were remelted several times to ensure homogeneity. The weight loss after the melting process was less than 0.5 weight %. The as-cast sample was wrapped in tantalum foil, sealed in an evacuated quartz tube and annealed at 1323 K for one week to improve the homogeneity and followed by quenching into cold water. The phase purity of the annealed sample was checked by performing powder X-ray diffraction (XRD) experiments at room temperature using $\text{Cu} - \text{K}_\alpha$ radiation of wavelength 1.54 Å on a Rigaku powder diffractometer. The obtained XRD pattern was analyzed by Rietveld refinement method using the FULLPROF software^{26,27}. Temperature dependence of magnetization ($M(T)$) and field dependence of magnetization ($M(H)$), were performed on a Physical Properties Measurement System (PPMS), Dynacool attached with a Vibrating Sample Magnetometer (VSM), Quan-

^{a)}Corresponding author

^{b)}Equal contributing author.

tum Design, USA. $M(T)$ was recorded in the standard process of zero-field cooled (ZFC) and field cooled (FC) mode followed by measurements in field cooled warm-up mode (FW). In ZFC modes, the sample was first cooled to $T = 2$ K in zero field, then a field was applied and thereafter the data were recorded while warming. In FC modes, the sample was first cooled to 2 K in the presence of an applied field and the data were recorded during warming in the same field. The ac-susceptibility ($\chi_{ac}(T)$) measurement was carried out under different frequency with a constant driven field of 3 Oe using same Dynacool system. The specific heat $C_P(T)$ measurement was carried out in the same Dynacool system using a thermal relaxation method in temperature range of 2–300 K. The temperature dependent resistivity $\rho(T)$ and isothermal field dependence of resistivity $\rho(H)$ were measured by the standard four-probe ac-method using the same apparatus.

B. Results and Discussion

1. Structural properties

Fig. 1 shows the Rietveld refinement of the powder x-ray diffraction (XRD) data obtained for Gd_2AgSi_3 performed using the centrosymmetric I_{41}/amd space group. It is confirmed that the compound crystallizes in α - ThSi_2 -type of tetragonal structure. The schematic representation of this structure is shown in the inset of Fig. 1. The crystallographic details obtained from the Rietveld refinement fit are given in table I.

The smallest Gd–Gd bond length in Gd_2AgSi_3 is 4.0929(1) Å. This value is larger than the expected Gd–Gd bond (atomic radii) of 3.5730 Å and therefore suggests a rather weak interaction between the rare-earth atoms. The shortest Gd–M (M = Ag + Si) bond was found to be 3.1226(1) Å. Similar values of RE–M bond (3.2508(2) Å for Ce_2AgGe_3 , 3.2311 Å for Pr_2AgGe_3 and 3.1996 Å for Nd_2AgGe_3)¹¹ have been reported for other 2–1–3 compounds forming in the same α - ThSi_2 crystal structure with same space group. Each Gd atom is surrounded by 10 M nearest neighbours atoms.

2. Magnetic properties

Fig. 2 shows the temperature variation of field-cooled dc-magnetic susceptibility ($\chi_{dc}(T) = M(T)/H$) of Gd_2AgSi_3 measured under an applied field of $H = 1.0$ T. Below 30 K, $\chi_{dc}(T)$ exhibits two anomalies. The expanded low-temperature region of $\chi_{dc}(T)$ is shown in the inset of Fig. 2 to highlight the double magnetic transition in Gd_2AgSi_3 . This double transition will be further investigated below.

The inverse magnetic susceptibility ($\chi_{dc}^{-1}(T)$) of the compound is presented on the right hand scale of Fig. 2. The $\chi_{dc}^{-1}(T)$ data below 300 K and 70 K can be described

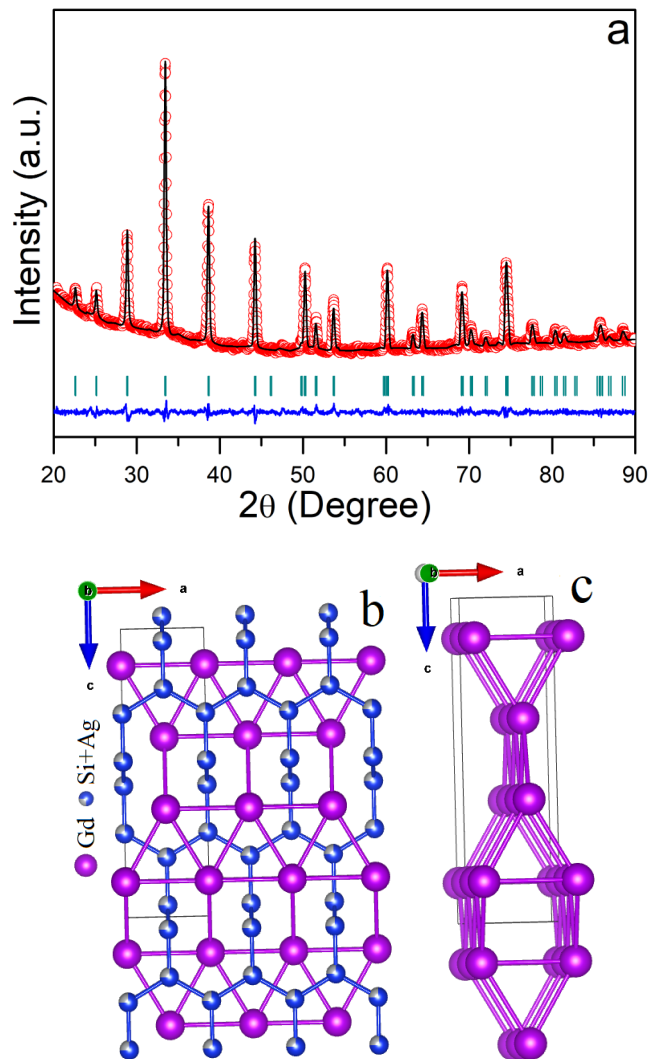


FIG. 1. (a): X-ray powder diffraction data for Gd_2AgSi_3 . Red symbols represent the experimental data and the black line represents the calculated data. The difference between experimental and calculated data is shown as blue line. A set of vertical bars represents the Bragg peak positions of the tetragonal α - ThSi_2 type structure. (b): The schematic representation of the tetragonal crystal structure of Gd_2AgSi_3 . (c): Gd atoms arrangement in the crystal structure.

using the Curie–Weiss law, $\chi_{dc} = C/(T - \theta_P)$, where C is the Curie constant proportional to the square of the effective magnetic moment (μ_{eff}) and θ_P is the paramagnetic Weiss temperature. The least-squares fit of the equation to the data leads to the values of $\mu_{\text{eff}} = 8.12 \mu_B/\text{Gd}$ and $\theta_P = -8$ K. The obtained μ_{eff} value is comparable to the theoretical free-ion value for Gd^{3+} ion which is $\approx 7.94 \mu_B/\text{Gd}$. The negative value of θ_P indicates that the dominant interactions in the compound are antiferromagnetic.

Two anomalies are found at low temperature, one at 20 K and another at 11 K. In order to get an insight into the two magnetic transitions, temperature depen-

TABLE I. The lattice parameters and unit cell volume Gd_2AgSi_3 compound obtained from the Rietveld refinement of XRD patterns for tetragonal phase along with the atomic coordinate positions.

a	4.094(2) Å
b	4.094(2) Å
c	14.178(2) Å
V	183.461(3) Å ³
R_p (%)	17.7
R_{wp} (%)	11.2
R_{exp} (%)	5.69
χ^2	4.74

Atomic coordinates for Gd_2AgSi_3

Atom	Wyckoff	x	y	z
Gd	4a	0	0.7500	0.1250
Ag	8e	0	0.2500	0.2925(1)
Si	8e	0	0.2500	0.2925(1)

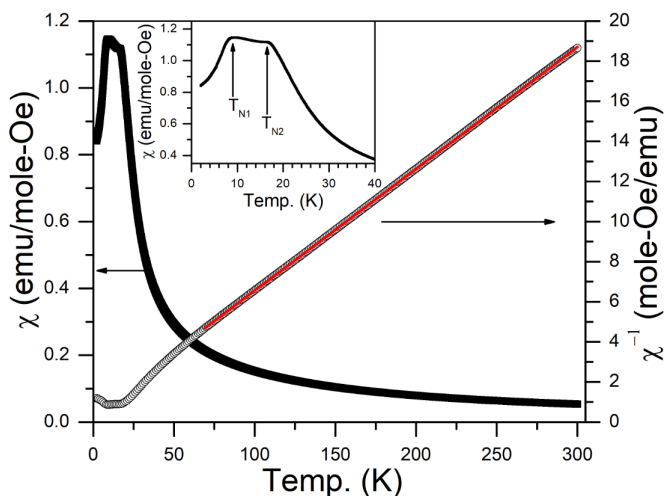


FIG. 2. Left scale: temperature dependence of dc-magnetic susceptibility ($\chi_{dc} = M/H$) of Gd_2AgSi_3 measured under a magnetic field of 1.0 T in FC mode. Right scale: inverse magnetic susceptibility as function of temperature for the same data. Inset: Expanded region at low temperatures of $\chi_{dc}(T)$ data showing two anomalies at $T_{N1} = 11$ K and $T_{N2} = 20$ K (see arrows).

dent magnetization of Gd_2AgSi_3 in ZFC and FC modes were measured at different applied magnetic fields and are represented in Fig. 3a – 3c. The two transitions show antiferromagnetic behavior with Néel temperatures $T_{N1} = 11$ K and $T_{N2} = 20$ K clearly visible in Fig. 3(a). One can also see from Fig. 3a, and 3b that the $M(T)$ shows an irreversibility behaviour between ZFC and FC magnetization. However, the relative magnitude of the bifurcation gradually decreases with increase in applied magnetic field and the two branches overlap for field values above 0.5 T.

Fig. 3(d) shows the real part of the $\chi_{ac}(T)$ data recorded at three different ac-field frequencies. The real component $\chi'_{ac}(T)$ of ac-susceptibility data confirm that the sample exhibits two magnetic transitions. However, there is no signature of spin glass behavior in the compound as the peaks in $\chi'_{ac}(T)$ data are frequency independent in the range of 500 to 9000 Hz.

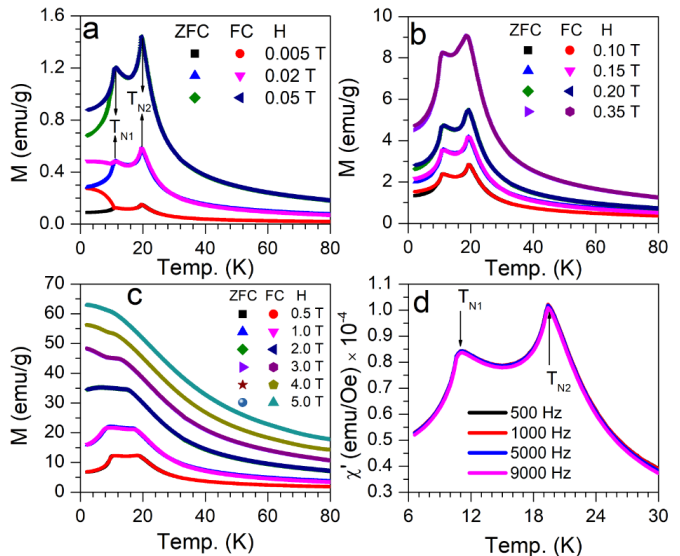


FIG. 3. (a)–(c): Temperature dependence of dc-magnetization measured under ZFC and FC protocols at different applied magnetic fields. (d): Temperature variation of the real part of ac-susceptibility measured at different ac-field frequencies with 3.0 Oe ac-driven field.

3. Specific heat

The temperature variation of specific heat ($C_P(T)$) of Gd_2AgSi_3 is presented in Fig. 4(a) along with its isostructural non-magnetic analogue La_2AgSi_3 (solid red line). Both compounds have C_P values close to the Dulong-Petit value of $3nR \approx 147$ J/mole-K, where n is the number of atoms in the formula unit and R is the universal gas constant. The compound La_2AgSi_3 exhibits a typical behavior for a non-magnetic metal between 2 K and 300 K.

The inset panel in Fig. 4(a) shows the expanded temperature region between 2 K and 30 K to highlight the double phase transition in Gd_2AgSi_3 . One can note that the low-temperature region of specific heat gives an evidence of two magnetic phase transitions with two nearby peaks at $T_{N1} \approx 11$ K and $T_{N2} \approx 20$ K, which is consistent with the peaks observed in $\chi(T)$ data. The $4f$ -magnetic contribution of specific heat (C_{4f}) was estimated by subtracting the zero-field specific heat for isostructural La_2AgSi_3 . The variation of C_{4f} as a function of temperature is shown in Fig. 4(a).

The magnetic entropy S_{4f} has been estimated using

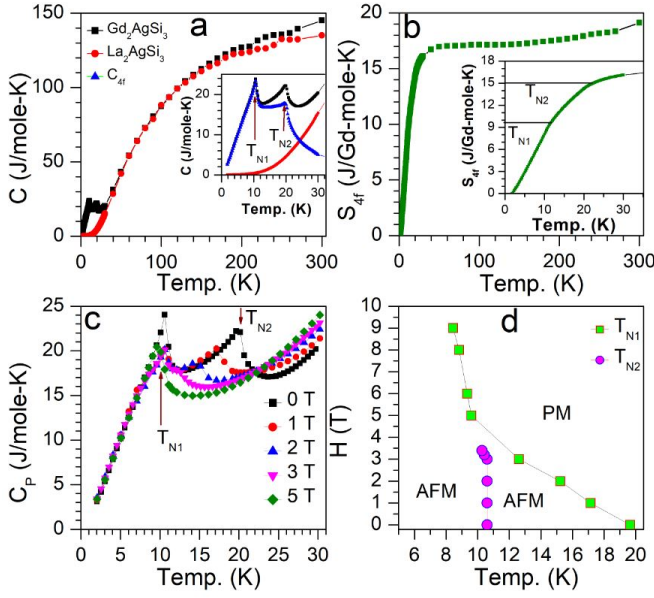


FIG. 4. (a): Zero-field specific heat (C_p) of Gd_2AgSi_3 in black symbols. The temperature dependence of zero-field specific heat of La_2AgSi_3 is represented as a red line. The magnetic contribution (C_{4f}) of specific heat is in blue symbols. Inset represents the expanded low-temperature region of C_p of Gd_2AgSi_3 , La_2AgSi_3 and C_{4f} of Gd_2AgSi_3 . (b): Temperature dependent magnetic entropy (S_{4f}). Inset represents the expanded low temperature region of S_{4f} . (c): The temperature dependence of C_p at different applied magnetic fields for Gd_2AgSi_3 . (d): Phase diagram for the variation of T_{N1} and T_{N2} with applied magnetic field.

the term $\int(C_{4f}/T)dT$. The variation of S_{4f} as function of temperature is shown in Fig. 4(b) and the expanded region at low temperature is shown in inset of Fig. 4(b). The magnetic entropy at T_{N1} is $S_{4f} \approx 9.6$ J/mole-Gd-K, and is $S_{4f} \approx 15$ J/mole-Gd-K at T_{N2} . Here, S_{4f} shows only $2/3$ of $R\ln(2S+1)$ is released at T_{N1} , while the entropy at T_{N2} is slightly less than that $R\ln 8$, which is expected for the full multiplet of Gd^{3+} .

The temperature dependence of C_p of Gd_2AgSi_3 was measured under different fields up to 5 T in the temperature range of 30 K to 2 K. Fig. 4(c) shows the C_p vs. T plots for different values of magnetic field. One can note from Fig. 4(c) that the peak at T_{N2} shifts to lower temperatures with increase in applied magnetic fields. This behavior is expected for an antiferromagnetic transition. However, the peak position at T_{N1} is not changing with fields up to 3 T. At a field value of 5 T, only one peak remains below T_{N1} which might shift marginally lower at this field and this transition evidently requires higher magnetic fields to be suppressed. The field vs. temperature phase diagram of Gd_2AgSi_3 derived from the field dependent specific heat measurement is shown in Fig. 4(d). The specific heat result indicates that the compound has a complex magnetic structure with two phase transitions.

4. Electrical resistivity

The zero-field electrical resistivity $\rho(T)$ of Gd_2AgSi_3 is shown in Fig. 5(a). The low-temperature region is expanded and shown in the inset of Fig. 5(a). The $\rho(T)$ gradually increases with temperature above 40 K. This indicates that the compound shows ordinary metallic behaviour in the paramagnetic region. However, $\rho(T)$ shows a broad minimum at $T \approx 35$ K and a maximum at $T \approx 8$ K before it decreases. The anomalies at below the transition temperature is possible for the superzone effects^{28,29}

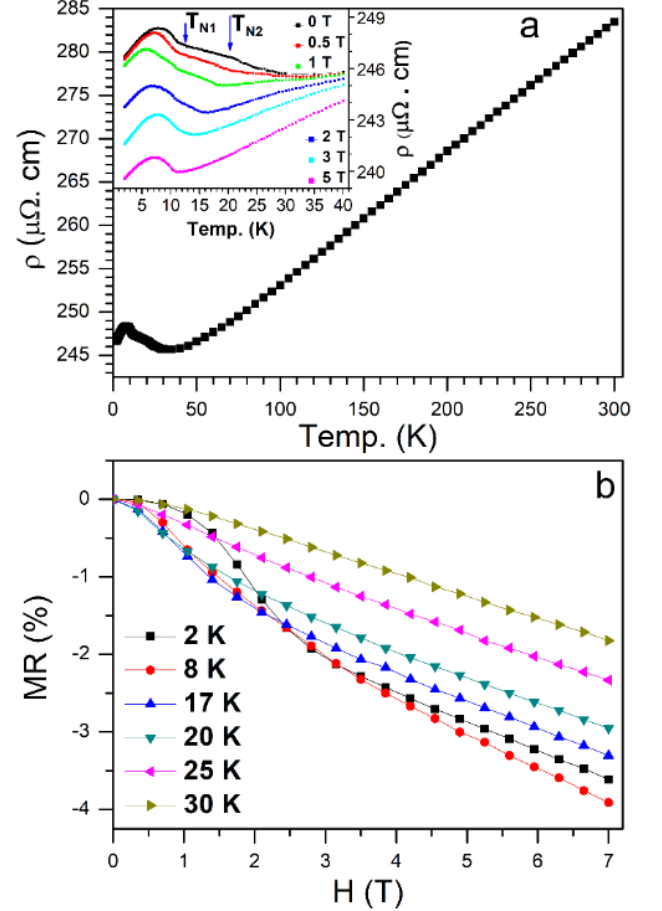


FIG. 5. (a): Temperature dependence of resistivity ($\rho(T)$) for Gd_2AgSi_3 in zero applied magnetic field. Inset: $\rho(T)$ was measured under different magnetic field in low temperature region. (b) Field dependence of the magnetoresistivity isotherms of Gd_2AgSi_3 .

Fig. 5a shows two kinks in $\rho(T)$ at about 21 K and 10 K (see arrows), marking the onset of magnetic ordering. These transition temperatures are consistent with the $\chi(T)$ and C_p results. It is also observed that the $\rho(T)$ does not drop immediately below either T_{N1} or T_{N2} , which would be expected due to the loss of spin-disorder scattering³⁰. This behavior highlights the complexity of the magnetic structure in this compound which also re-

flects from the formation of superzone boundary gaps in some portions of the Fermi surface²⁸. The inset of Fig. 5(a) shows the $\rho(T)$ of Gd_2AgSi_3 for different values of applied magnetic fields. As seen in the inset panel of Fig. 5a, both the transition temperatures T_{N_1} and T_{N_2} are getting suppressed with increase in magnetic field, which is commonly seen in antiferromagnetic materials. However, the superzone feature remains visible upto 5 T. It can also be noted that $\rho(T)$ decreases with increasing magnetic field which indicates a negative magnetoresistance (MR) feature³⁰.

In order to obtain the magnetic field dependent magnetoresistance (MR), isothermal field dependent resistivity measurements were carried out at different temperature in the range of 2 K to 30 K. MR was estimated by using the following formula:

$$\text{MR} = \frac{\rho(H, T) - \rho(0, T)}{\rho(0, T)} \times 100\%, \quad (1)$$

where $\rho(0, T)$ is the resistivity at zero magnetic field and $\rho(H, T)$ is the resistivity at applied field 'H'. Fig. 5(b) shows the nature of field dependent MR. It is apparent from Fig. 5(b) that Gd_2AgSi_3 exhibits negative MR over a wide range of temperature. Negative MR is also reported on other rare-earth based antiferromagnetic compound^{28,30–33}.

5. Magnetocaloric effect

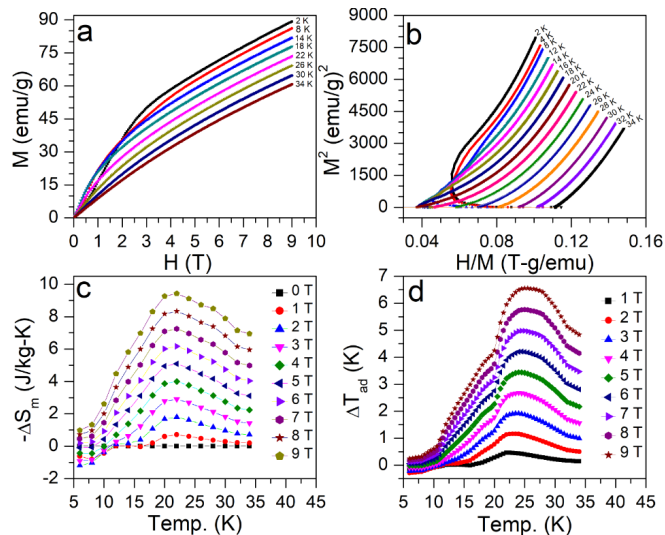


FIG. 6. (a): Isothermal magnetization during magnetic field change 0 T \rightarrow 9 T of Gd_2AgSi_3 at different temperatures between 2 K and 34 K with a step of 2 K. (b) Arrott plots (M^2) vs. H/M at different temperatures. (c) Temperature variation of magnetic entropy change (ΔS_m) for different fields. (d) Variation of adiabatic temperature change as a function of temperature for different fields.

In order to obtain the isothermal magnetic entropy

changes for MCE study and for more confirmation about order of magnetic phase transition, isothermal magnetization for different temperatures has been measured for Gd_2AgSi_3 . There was no hysteresis loop at 2 K (not shown), which confirmed that the compound shows soft magnetic behavior. Fig. 6(a) shows magnetization as function of field $M(H)$ at different temperatures between 2 K and 34 K with a step of 2 K for field cycle 0 T \rightarrow 9 T. The spontaneous magnetic moment of Gd_2AgSi_3 at 2 K for a field of 9 T is $5.6 \mu_B/\text{Gd}^{3+}$, which is less than the spontaneous magnetization of free Gd^{3+} ($gJ = 7\mu_B$) moments. One can see that isothermal M–H shows a typical metamagnetic behaviour below T_{N_1} . The critical magnetic field was determined from the maximum of dM/dH and found to be 0.9 T for 2 K. The Arrott–plots (M^2 vs. H/M) was derived from the isothermal $M(H)$ curves to investigate the nature of the phase transitions. Fig. 6(b) depicts the Arrott plot for Gd_2AgSi_3 compound. Based on the Banarjee criterion³⁴, the M^2 vs. H/M plots show negative slopes as a function of magnetic field, indicating a first-order magnetic phase transition.

TABLE II. The transition temperature, the maximum values of magnetic entropy change (ΔS_M), and refrigeration capacity (RC) under the field change of 0–5 T for some rare-earth compounds of $\text{RE}_2\text{T}_2\text{X}$.

Method	T_N/T_C (K)	$-\Delta S_M$ (J/kg.K)	RC (J/kg)	Ref
Gd_2NiSi_3	16.4	≈ 13	$\approx 300^*$	9
$\text{Gd}_2\text{ZnMnO}_6$	6.4	15.17	226.2*	17
TmZn	8.4	26.9	214	39
HoPdIn	23/6	14.6	374	40
Ho_3Rh_2	23	14.1	382	41
$\text{GdCo}_2\text{B}_2\text{C}$	17.2	10.3	238*	42
$\text{Gd}_2\text{Rh}_3\text{Ge}$	64	9.4	352*	43
$\text{Ho}_2\text{FeAlO}_6$	<2	7.1	144.5	44
$\text{Pr}_2\text{Ni}_{0.95}\text{Si}_{2.95}$	3.3	≈ 6	—	45
Gd_2AgSi_3	20	5.1	103	This work

* represents for RCP.

Double phase magnetic materials are interesting for MCE as they show a wide range of maximum magnetic entropy change (ΔS_m^{max})^{35,36}. The broad behaviour of ΔS_m^{max} are beneficial for the application of magnetic refrigeration^{35–37}. Hence, the MCE of Gd_2AgSi_3 has been investigated and the values of ΔS_m have been calculated from magnetization isotherms using the Maxwell's thermodynamic relation¹⁶:

$$\Delta S_m(T, H) = \int_0^H \left(\frac{\partial M}{\partial T} \right) dH. \quad (2)$$

Fig. 6(c) shows the temperature dependence of $-\Delta S_m$ for the change of magnetic field up to 9 T. The negative values of $-\Delta S_m$ below T_{N_2} for small magnetic field

change is possible for the antiferromagnetic ground state of Gd_2TX_3 . Positive value of $-\Delta S_m$ at the relatively large magnetic field ($H > 5$ T) was observed for the possibility of field-induced antiferromagnetic-ferromagnetic metamagnetic transition³⁸. The $-\Delta S_m$ vs. T graph shows a peak at around the magnetic transition temperature T_{N_2} . Here, we have observed a single peak instead of two peaks, which might be possible due to the presence of a metamagnetic behavior upto first transition. A maximum value of $-\Delta S_m^{max} = 9.5$ J/kg-K is found around the transition temperature T_{N_2} at a change of magnetic field of 9 T. The observed value is compared with other reported values in Table II.

ΔT_{ad} was evaluated from both $-\Delta S_m(T, H)$ and the zero-field specific heat data using the relation:^{21,22}

$$\Delta T_{ad}(T, H) = -\frac{T\Delta S_m}{C_p(T, H)}. \quad (3)$$

The peak value of ΔT_{ad} is 7.5 K for a field change of 9 T, as shown in Fig. 6(d).

For a refrigeration cycle, the amount of heat transferred from hot to cold sinks can be estimated by the cooling power per unit volume, simply known as RC and RCP. The RC and RCP can be evaluated from $-\Delta S_m$ vs T curve using the mathematical formula $RC = \int_{T_1}^{T_2} |\Delta S_m| dT$ and $RCP = |-\Delta S_m^{max}| \times \delta T_{FMHM}$, respectively^{20,23,37}. Here, T_1 and T_2 are the temperatures corresponding to the left and right sides of the half maximum $-\Delta S_m$ peak. δT_{FMHM} is the full width at half maximum for each field. The obtained values of RC (RCP) are found to be as large as 103(140) J/kg and 302(415) J/kg for the changes of magnetic field 0–5 T and 0–9 T, respectively. The obtained values of Gd_2AgSi_3 are compared in Table II. As seen from Table II, the obtained MCE parameters of Gd_2AgSi_3 are quite small in comparison with other reported MCE materials.

C. Summary

In summary, we have experimentally studied the crystal structure, magnetic, transport, magnetoresistance and magnetic cooling properties of a new stoichiometric compound Gd_2AgSi_3 . This polycrystalline sample successfully formed as a single phase in a tetragonal α - ThSi_2 -type crystal structure with space group I_{41}/amd . Magnetic susceptibility, electrical resistivity and specific heat measurements reveal that the compound exhibits two antiferromagnetic transitions at 11 K and 20 K. The superzone effect from resistivity is observed at below the transition temperature. From field dependent isotherm resistivity characterization, it is confirmed that the compound possess negative magnetoresistance in the both antiferromagnetic ordered and paramagnetic region. The magnetic field induced first-order magnetic transitions in the magnetically ordered state is confirmed from the

Arrott-plots. MCE of this present compound is systematically studied and the obtained values are compared with other reported compounds. These results contribute towards a better understanding of this class of materials.

Acknowledgements

This work is supported by Global Excellence and Stature (UJ-GES) fellowship, University of Johannesburg, South Africa. DFR thanks OWSD and SIDA for the fellowship towards PhD studies. AMS thanks the URC/FRC (935A9) of UJ for assistance of financial support.

References

- ¹E. Khamitcaeva, A. Tursina, A. Gribanov, D. Gnida, P. Wisniewski, and D. Kaczorowski, *J. Alloys. Compd.* 708 (2017) 162–168.
- ²Z.Y. Pan, C.D. Cao, X.J. Bai, R.B. Song, J.B. Zheng, and L.B. Duan, *Chin. Phys. B.* 22 (2013) 056102.
- ³M. Smidman, C. Ritter, D. T. Adroja, S. Rayaprol, T. Basu, E. V. Sampathkumaran, and A. D. Hillier, *Phys. Rev. B.* 100 (2019) 134423.
- ⁴D. Kaczorowski, A. V. Gribanov, S. F. Dunaev, and E. V. Marushina, *Intermetallics* 95 (2018) 130–136.
- ⁵S.C. Peter, U. Subbarao, S. Sarkar, G. Vaitheeswaran, A. Svane, and M.G. Kanatzidis, *J. Alloys. Compd.* 589 (2014) 405.
- ⁶S. Pakhira, R. Ranganathan, and C. Mazumdar, *J. Magn. Mater.* 512 (2020) 167055.
- ⁷S.C. Peter, M. Chondroudi, C.D. Malliakas, M. Balasubramanian, and M. G. Kanatzidis, *J. Am. Chem. Soc.* 133 (2011) 13840–13843.
- ⁸L. S. Litzbarski, T. Klimczuk, and M. J. Winiarski, *J. Phys. Condens. Matter* 32 (2020) 225706.
- ⁹S. Pakhira, C. Mazumdar, R. Ranganathan, S. Giri, and Maxim Avdeev, *Phys. Rev. B.* 94 (2016) 104414.
- ¹⁰V.H. Tran, *J. Phys.: Condens. Matter* 8 (1996) 6267.
- ¹¹S. Sarkar, D. Mumbaraddi, P. Halappa, D. Kalsi, S. Rayaprol, and S. Peter, *J. Solid State Chem.* 229 (2015) 287–295.
- ¹²Z. Wang, Y. Su, S.Z. Lin, and C.D. Batista, *Phys. Rev. Lett.* 124 (2020) 207201.
- ¹³S. Pakhira, C. Mazumdar, R. Ranganathan, S. Giri, and M. Avdeev, *Phys. Rev. B.* 94 (2016) 104414.
- ¹⁴Z. J. Mo, J. Shen, X. Q. Gao, Y. Liu, C. C. Tang, J. F. Wu, F. X. Hu, J. R. Sun, and B. G. Shen, *J. Alloys. Compd.* 626 (2015) 145–149.
- ¹⁵Y. Zhang, D. Guo, Y. Yang, S. Geng, X. Li, Z. Ren, and G. Wilde, *J. Alloys. Compd.* 702 (2017) 546–550.
- ¹⁶A.M. Tishin and Y.I. Spichkin, *The Magnetocaloric Effect and its Application* (CRC Press) (2016).
- ¹⁷L. Li, P. Xu, S. Ye, Y. Li, G. Liu, D. Huo, and M. Yan, *Acta Mater.* 194 (2020) 354–365.
- ¹⁸V. Franco, J. S. Blázquez, J. J. Ipus, J. Y. Law, L. M. Moreno-Ramírez, and A. Conde, *Prog. Mater. Sci.* 93 (2018) 112–232.
- ¹⁹L. Li, and M. Yan, *J. Alloys. Compd.* 823 (2020) 153810.
- ²⁰L. Li, *Chin. Phys. B.* 25 (2016) 037502.
- ²¹J.L. Wang, S.J. Campbell, J.M. Cadogan, A.J. Studer, R. Zeng, and S.X. Dou, *Appl. Phys. Lett.* 98 (2011) 232509.
- ²²M.F. Md. Din, J.L. Wang, S.J. Campbell, A.J. Studer, and M. Avdeev, *Appl. Phys. Lett.* 104 (2014) 042401.
- ²³Y.X. Wang, H. Zhang, M.L. Wu, K. Tao, Y.W. Li, T. Yan, K.W. Long, T. Long, Z. Pang, and Y. Long, *Chin. Phys. B* 25 (2016) 127104.

- ²⁴V. K. Pecharsky and K. A. Gschneidner, Jr., *Phys. Rev. Lett.* 78 (1997) 4494.
- ²⁵V. K. Pecharsky and K. A. Gschneidner, Jr., *Appl. Phys. Lett.* 70 (1997) 3299.
- ²⁶Rietveld H. M., *J. Appl. Crystallogr.* 2 (1969) 65.
- ²⁷Rodriguez-Carvajal J., Fullprof Suite <http://www.ill.eu/sites/fullprof/> (2017).
- ²⁸S.R. Saha, H. Sugawara, T.D. Matsuda, and H. Sato, *Phys. Rev. B* 60 (1999) 12162.
- ²⁹S. Ramakrishnan, K. Ghosh, and G. Chandra, *Phys. Rev. B* 45 (1992) 10769.
- ³⁰J.Y. Chan, S.M. Kauzlarich, P. Klavins, R.N. Shelton, and D.J. Webb, *Phys. Rev. B* 57 (1998) R8103.
- ³¹O. Pavlosiuk, D. Kaczorowski, and P. Wisniewski, *Phys. Rev. B* 99 (2019) 125142.
- ³²H. C. Chen, Z. F. Lou, Y. X. Zhou, Q. Chen, B. J. Xu, S. J. Chen, J. H. Du, J. H. Yang, H. D. Wang, and M. H. Fang, *Chin. Phys. Lett.* 37 (2020) 047201.
- ³³M. H. Jung, A. H. Lacerda, and T. Takabatake, *Phys. Rev. B* 65 (2002) 132405.
- ³⁴S.K. Banerjee, *Phys. Lett.* 12 (1964) 16.
- ³⁵L. Li, Y. Yuan, Y. Qi, Q. Wang, and S. Zhou, *Mater. Res. Lett.* 6, no. 1 (2018): 67–71.
- ³⁶G. Li, J. Wang, Z. Cheng, Q. Ren, C. Fang, and S. Dou, *Appl. Phys. Lett.* 106, (2015) 182405.
- ³⁷L. Li, O. Niehaus, M. Kersting, and R. Pöttgen, *Appl. Phys. Lett.* 104 (2014) 092416.
- ³⁸Y.H. Ding, F.Z. Meng, L.C. Wang, R.S. Liu, and J. Shen, *Chin. Phys. B* 29 (2020) 077501.
- ³⁹L. Li, Y. Yuan, Y. Zhang, T. Namiki, K. Nishimura, R. Pöttgen, and S. Zhou, *Appl. Phys. Lett.* 107 (2015) 132401.
- ⁴⁰L.W. Li, T. Namiki, D.X. Huo, Z.H. Qian, and K. Nishimura, *Appl. Phys. Lett.* 103 (2013) 222405.
- ⁴¹Y. J. Wang, Y. S. Du, Y. Q. Zhang, L. Li, L. Ma, J. Wang, J. T. Zhao, and G. H. Rao, *Intermetallics* 127 (2020) 106989.
- ⁴²Y. Zhang, D. Guo, B. Wu, H. Wang, R. Guan, X. Li, and Z. Ren, *J. Alloys Compd.* 817 (2020) 152780.
- ⁴³B. Sahu, J. Y. Law, A. M. Strydom, V. Franco, and H. S. Nair, *J. Magn. Magn. Mater.* 514 (2020) 166988.
- ⁴⁴B. Wu, Y. Zhang, D. Guo, J. Wang, and Z. Ren, *Ceram. Int.* 47 (2021) 6290–6297.
- ⁴⁵S. Pakhira, C. Mazumdar, and R. Ranganathan, *Intermetallics* 111 (2019) 106490.